Multiphase Cage-Rotor Induction-Machine Drive With Direct Implementation of Brush DC Operation

Nkosinathi Gule, *Member, IEEE*, and Maarten J. Kamper, *Senior Member, IEEE*

***Abstract*—In this paper, a multiphase induction-machine drive utilizing the brush-dc-machine operation principle is presented and implemented on a cage-rotor multiphase induction machine. The results from measurements prove that the proposed brush dc control method for multiphase induction-machine drives produces remarkable results in the subbase and flux-weakening-speed regions of the drive. Also, results show that the drive system's efficiency compares well with that of a standard three-phase drive system. The method can be used for any high-phase-number cage or wound-rotor induction machine.**

***Index Terms*—Induction-machine control, multiphase.**

I. Introduction

MULTIPHASE induction-machine drives possess several advantages over conventional three-phase induction-machine drives in high-power applications [1]–[10]. Aside from better fault tolerance and higher reliability, the advantages of multiphase induction machines include reductions in amplitude of torque pulsation, rotor harmonic currents, current per phase without increasing the phase voltage and dc-link current harmonics, increases in the machine power and torque per rms current for the same volume machine, and an increase in the torque pulsation frequency. Depending on the stator winding, other advantages are independent control of multimotor multiphase drive systems with a single power electronic converter supply and torque enhancement through stator current harmonic injection [4], [8]. Also, a higher phase number leads to the improvement of the quality of the air-gap flux-density waveform regardless of the current waveform or winding design, because with a higher phase number, there is less interaction between space and time harmonics.

At present, multiphase induction machines are used in highly specialized applications such as locomotive traction, electric and hybrid-electric vehicles, industrial high-power applications, electric ship propulsion [5], [11], and other electric aircraft [12]–[14]. Battery-powered applications such as cordless power tools and small traction drives are also considered [15].

Manuscript received November 28, 2011; revised March 5, 2012; accepted April 23, 2012. Date of publication October 23, 2012; date of current version December 31, 2012. Paper 2011-IDC-663.R1, presented at the 2011 IEEE International Electric Machines and Drives Conference, Niagara Falls, ON, Canada, May 15–18, and approved for publication in the IEEE TRANSACTIONS ON INDUSTRY APPLICATIONS by the Industrial Drives Committee of the IEEE Industry Applications Society.

The authors are with the Department of Electrical and Electronic Engineering, Stellenbosch University, Stellenbosch 7602, South Africa (e-mail: nathie@sun.ac.za; kamper@sun.ac.za).

Color versions of one or more of the figures in this paper are available online at http://ieeexplore.ieee.org.

Digital Object Identifier 10.1109/TIA.2012.2226195

The speed-control methods of multiphase induction-machine drives are similar to those of three-phase induction-machine drives. Scalar control has lost popularity, while more interest has now been shown in vector and direct torque (DTC) controls due to the higher cost of multiphase power electronics compared with that of implementing control algorithms [4]. However, currently employed control techniques are quite complex as the coordinate transformations and model representations of multiphase induction machines have become more demanding [1], [4].

Recently, a control method that does not require any coordinate transformation for a six-phase wound-rotor induction-machine drive was proposed and evaluated [16]. This control method is, in effect, a direct implementation of the operation of a brush dc machine with compensating windings, i.e., by using the stator-phase windings to act alternately as flux- or torque-producing phases. This control method is proved from practical measurements on a two-pole six-phase wound-rotor induction-machine drive. In this paper, this control method is termed the "brush dc equivalent" (BDCE) control method.

In this paper, the machine drive and control method of [16] is further investigated and evaluated on an 11-kW nine-phase cage-rotor induction-machine drive. The measurement results of the BDCE-controlled nine-phase induction-machine drive in the subbase and flux-weakening-speed regions of the drive are given. Also, the drive system's (converter and induction machine) efficiency is measured and compared with that of a standard three-phase drive system. The application of this type of drive is only for very high power variable-speed drive applications, e.g., in the 50-MW power level.

II. BDCE Method

The conceptualization of the BDCE control method is described in this section since the BDCE control method is relatively new. The operation principle of BDCE control and a simple analytical method of finding the static torque of a BDCE-controlled multiphase induction machine are also presented in this section.

A. Conceptualization of the BDCE Operation of the Multiphase Induction Machine

A dc machine with a salient stator (field poles) can be transformed to a round-stator concentrated winding machine, as shown in Fig. 1. In the figure, the field and compensating windings (of the dc machine) are shifted and distributed in slots around the round stator. This transformed dc machine can be

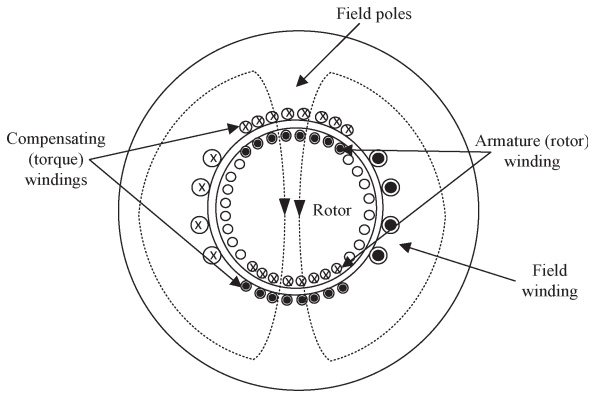

Fig. 1. Geometry of a round rotor machine with field and compensating windings in a round stator.

converted to a multiphase induction machine through a proper winding layout and appropriate stator-current waveforms as explained in the following.

In the multiphase induction machine, the compensating (or torque) windings are replaced with individual coils that become a group of torque phases, and also, the field windings are replaced with independent coils that become a group of field phases, as shown in Fig. 1. All the coils (field and torque) are placed in evenly spaced identical slots on a nonsalient round stator, and the number of turns is maintained the same in all the stator slots. The armature winding is replaced with a cage (or wound-rotor) winding.

For the induction machine to operate, a smooth rotating air-gap flux is required. Thus, stator-current waveforms and a stator-winding layout that allows for a phase to alternate between being field- and torque-producing phases are constructed. This is done such that, at each time instance, a group of phases acts as field-producing phases and the rest as torque-producing phases. From this, it can be seen that the moving rotating air-gap flux-density waveform produced by the field-producing phases is quasi-squarelike.

The flux produced by the field-producing phases leads to induced voltages at slip speed in the rotor bars located under the torque phases. Then, the rotor-phase currents will flow in the cage or shorted wound-rotor winding under the torque phases and produce a flux in quadrature to the main flux. The torque current flowing in the torque phases must then produce a countermagnetomotive force (MMF) to balance the MMF produced by the rotor current; this is similar to the compensating winding in dc machines. Thus, torque in the machine is produced similarly as in dc machines with compensating windings.

B. Constructing the Stator-Current Waveforms for BDCE Control

A general procedure for constructing the current waveforms for BDCE-controlled machines with a number of phases which are multiples of three can be developed. To ensure smooth rotating stator-torque and stator-field MMFs, a trapezoidal-shaped stator-phase current waveform is used, as shown in Fig. 2. In this figure, the numbers of field m_f and torque m_t phases are

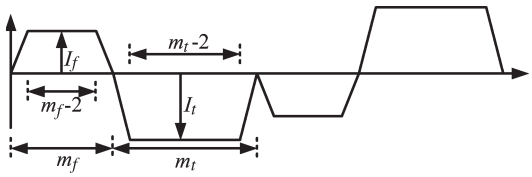

Fig. 2. Trapezoidal stator-current waveform.

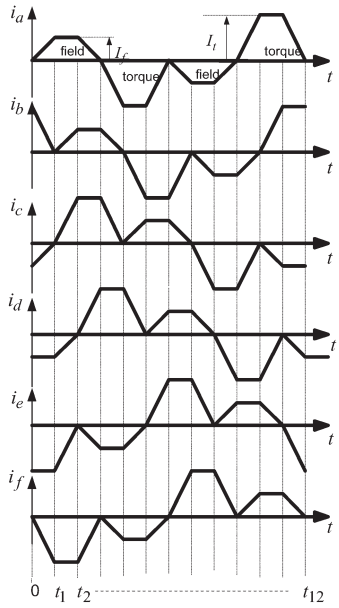

Fig. 3. Trapezoidal six-phase current waveforms [16].

labeled. The sum of m_f and m_t gives the total number of stator phases for the machine N_p, i.e., $N_p = m_f + m_t$. I_f and I_t are the amplitudes of the field and torque currents, respectively, and they are calculated once the rating of the machine is known.

For a machine with N_p stator phases, the phases are grouped into three groups of $N_p/3$ phases each. Then, the appropriate combination of m_f and m_t is selected through the method described in [17], and the waveform, as shown in Fig. 2, is constructed.

All the other phases are constructed by phase shifting this waveform by

$$\varphi = \frac{2\pi}{3}(z-1) + \frac{\pi}{N_p}(i-1) \tag{1}$$

where φ is the phase shift, z is the group index, $z = 1, 2,$ or 3, and i is the phase index, i.e., $i = 1, 2, \ldots, N_p/3$.

C. Operation Principle of the BDCE-Controlled Induction Machine

The principle of operation of the BDCE multiphase induction-machine drive is best explained graphically. The configuration of the stator-phase current waveforms shown in Fig. 3 allows a separate rotating flux or field MMF with an amplitude F_f and a torque MMF with an amplitude F_t in a two-pole six-phase induction machine. As in Fig. 2, the stator-phase current consists of trapezoidal-shaped field and torque current components, with flat-topped amplitudes of I_f and I_t,

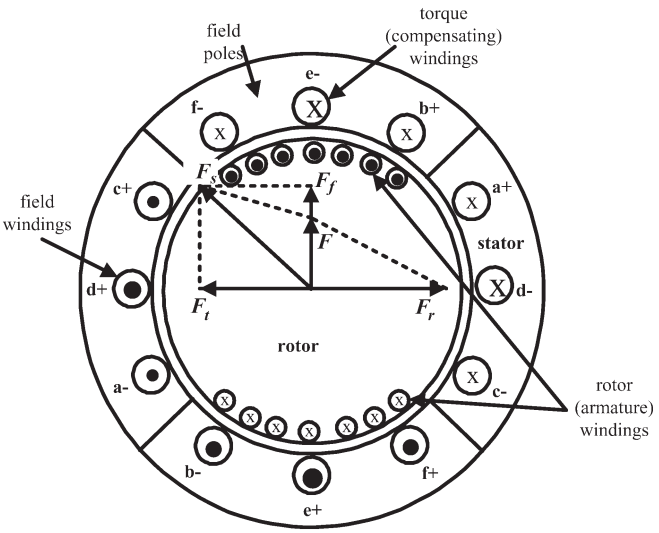

Fig. 4. Current distribution and MMF space phasors at time $t = t_1/2$ of the waveforms in Fig. 3.

respectively. That is, a stator phase acts alternately in time as either a flux- or a torque-producing phase. Furthermore, it can be seen from Figs. 3 and 4 that, at any instant, there are always three neighboring stator-phase windings that act as field windings to generate the flux in the machine while the other three neighboring stator-phase windings always act as torque windings to generate the torque of the machine. The generated flux in the machine will lead to induced rotor-phase voltages and currents at slip speed. The rotor currents produce the rotor MMF F_r. The torque current flowing in the torque-producing stator phases, however, produces a counter-MMF that balances the rotor MMF during the operation of the BDCE-controlled multiphase induction machine. Thus, as shown in Fig. 4, with $F_t = F_r$, the balanced MMF condition (flux-decoupling condition) is achieved. There is, thus, an important relationship between the torque current I_t and the angular slip frequency ω_{sl} for balanced MMF control (or decouple control), that is

$$k = \frac{\omega_{sl}}{I_t}. \tag{2}$$

The relationship given by (2) is used in the control system, where k is used as a control gain. The control gain k also depends on the physical dimensions of the machine, total number of phases, rotor-phase resistance, and air-gap flux density, as discussed in the next section.

Fig. 5 shows a block diagram of an N_p-phase induction-machine drive under flux and torque control. Similarly to [18] and phase-redundant multiphase systems [2], a full-bridge inverter is used for each stator-phase winding, which results in $2N_p$ phase legs for an N_p-phase drive. The full-bridge inverter allows for the separate control of each phase since each phase alternates as a torque- or a flux-producing phase. The rotor speed, together with the phase currents of the drive, are measured and fed back to a digital-signal-processor (DSP) controller. The flux, and hence, the field current, is kept constant under base speed. The speed controller controls the torque-command current I_t^* from which the slip angular frequency ω_{sl} is determined using the control gain k of (2). From this and from the known field-command current I_f^*, the N_p reference phase currents of the drive are generated. In this case, a digitally implemented hysteresis current regulator, using a field-programmable gate array, is used for the current control. The switching signals are sent to the inverter via fiber optic cables. The advantage of this control method is that it does not require any transformations and model representations such as in vector control and DTC. Also, from Fig. 5, it can be seen that the BDCE control method does not depend on the rotor position.

D. Analysis of a BDCE-Controlled N_p-Phase Induction Machine

From Figs. 1–3, it is clear that, at any time instance, the amplitude of the field MMF F_f is

$$F_f = (m_f - 1)N_s I_f \tag{3}$$

where N_s is the number of turns in series per phase. Note that the expression given in (3) applies to any BDCE-controlled induction machine with any number of phases. Similarly, the amplitude of the torque MMF is

$$F_t = (m_t - 1)N_s I_t. \tag{4}$$

In the analysis, assuming perfect commutation and quasi-square-wave air-gap flux density, the induced rotor-phase current waveform will have an ideal squarelike form, as shown in Fig. 6. With the position of the active rotor-phase windings opposite the position of the compensating or torque phase windings of the stator, the rotor MMF amplitude is given by

$$F_r = m_{\mathrm{ra}} N_r I_r \tag{5}$$

where m_{ra} is the number of active bars or rotor phases underneath a pole at any time instance and N_r is the number of turns in series per rotor phase ($N_r = 0.5$ for a cage rotor).

Theoretically, the number of active bars per pole is

$$m_{\mathrm{ra}} = \frac{M_r(m_t - 1)}{2N_p p} \tag{6}$$

where M_r is the number of rotor bars, m_t is the number of torque phases, $N_p = m_t + m_f$, and p is the number of pole pairs.

The rotor-phase winding or bar-induced voltage waveform assumes a near square due to the quasi-square air-gap flux density. The flat-topped amplitude of this waveform can be calculated similarly to that of dc machines as

$$E_b = 2N_r B l \omega_{sl} r_g \tag{7}$$

where ω_{sl} is the angular slip frequency, B is the air-gap flux density, l is the stack length, and r_g is the air-gap radius. The induced rotor-bar current is given by

$$I_r = \frac{E_b}{R_b} = \frac{2N_r B l \omega_{sl} r_g}{R_b} \tag{8}$$

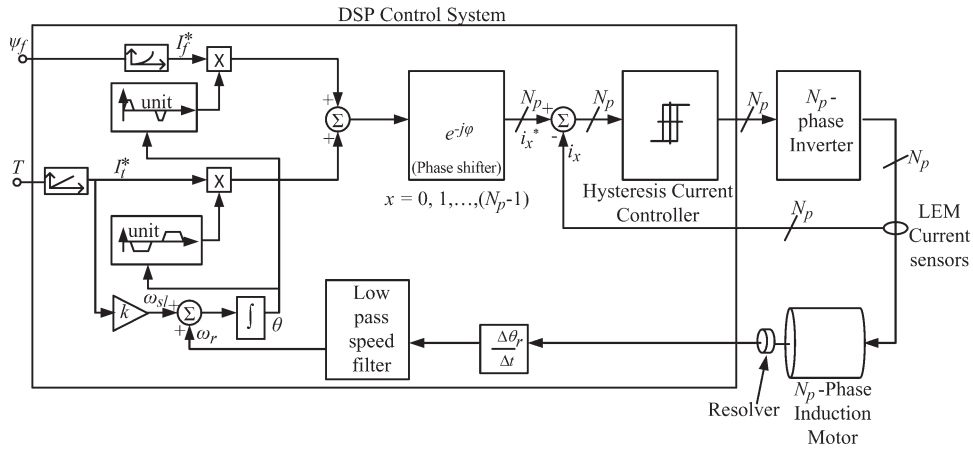

Fig. 5. BDCE control system of an N_p-phase induction motor.

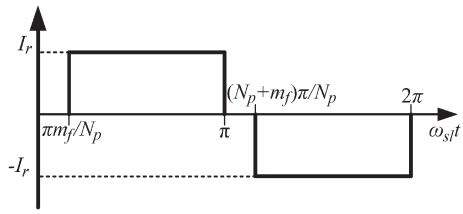

Fig. 6. Assumed rotor-bar current waveform of a BDCE-controlled N_p-phase induction machine.

where R_b is the rotor-phase resistance. Using the Lorentz force law, similarly to the brush-dc-machine case, the electromagnetic torque of the machine is given by

$$T = 2m_{\rm ra}N_r r_g l B I_r. \tag{9}$$

Under balanced MMF conditions $(F_t = F_r)$, using (4), (5), and (9), it can be shown that

$$T = 2(m_t - 1)N_s r_g l B I_t. \tag{10}$$

Thus, there is a linear relationship between torque and torque current I_t similar to the linear relationship between torque and armature current in dc machine theory.

Considering MMF balance, the control gain can be evaluated from (2), (4), (5), and (8) as

$$k = \frac{\omega_{sl}}{I_t} = \frac{(m_t - 1)N_s R_b}{2m_{\rm ra}N_r^2 B l r_g}. \tag{11}$$

It is clear that k depends on the bar resistance R_b (which, in turn, is dependent on temperature) and the air-gap flux density B. B can be controlled through the field current I_f.

III. Nine-Phase Cage-Rotor Induction-Machine-Drive Evaluation

A nine-phase cage-rotor induction-machine drive is developed using the proposed control method of Section II. A cage rotor is specifically selected in this case as [16] uses a wound rotor—it is important to know if additional copper loss is generated in the cage rotor due to the trapezoidal stator currents.

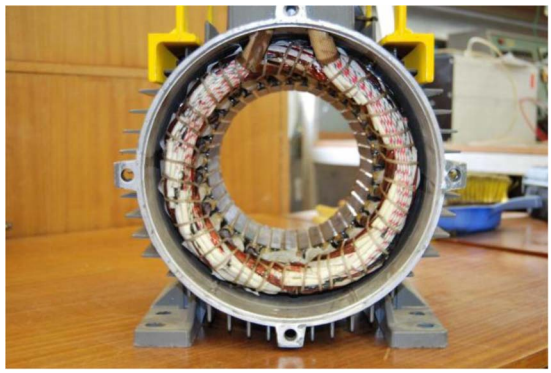

Fig. 7. Stator of the nine-phase induction machine.

TABLE I
Machine Parameters of a Four-Pole Nine-Phase Induction Machine

Rated Power, P_n	11kW
Air-gap length, g	0.5 mm
Stack length, l	127 mm (copper bars)
Stator radius	130 mm
Rotor radius, r_g	84.5 mm
End ring segment resistance, R_e	1.28e-6 Ω (75°C)
End ring segment inductance, L_{er}	29.2 nH
Number of field phases, m_f	3
Number of torque phases, m_t	6
Number of rotor bars, M_r	28
Number of stator slots, M_s	36
Number of series turns per stator phase, N_s	170
Air-gap flux density, B	0.7 T
Rated I_f	5.83 A
Rated I_t	5.5 A
Rated k	0.638 rad/As
Rated speed	1466 r/min

A standard 11-kW four-pole 36-slot three-phase induction-machine stator is rewinded to a nine-phase stator with full-pitch (concentrated) coils. The rewinded stator image is shown in Fig. 7. The original 28-slot cast aluminum cage rotor of

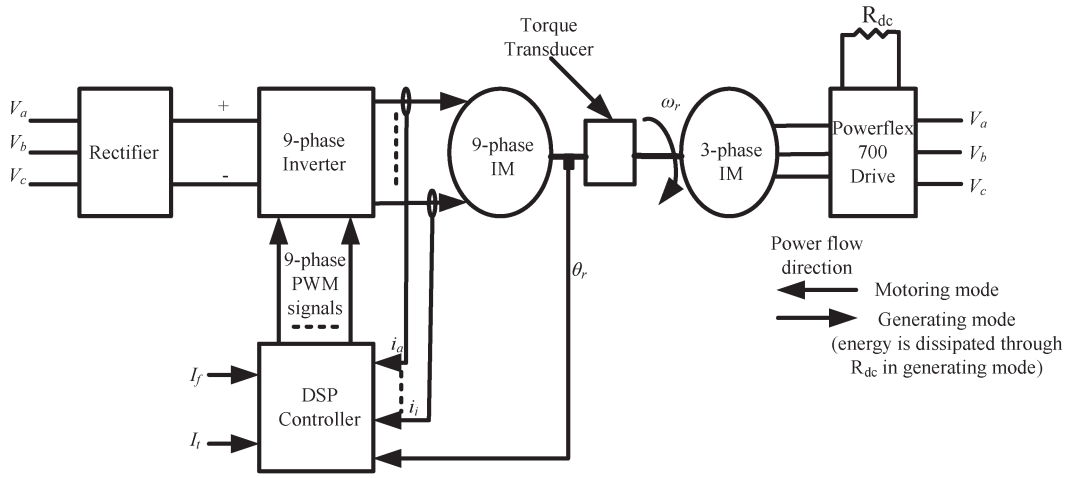

Fig. 8. Schematic of the test setup.

the three-phase induction machine is used for the rotor of the nine-phase induction machine. The additional parameters of the nine-phase machine are given in Table I.

The nine-phase inverter comprises of intelligent power modules (IPMs), the control and isolated power circuits, the dc bus bar, and per-phase current sensors. A modular design is utilized in the design of the inverter since it allows for independent testing and simple replacement of faulty boards. An H-bridge is required for each phase of the nine-phase machine; thus, the inverter consists of six 6MBP25RA120 three-phase IPMs. Each control board is shared by two IPMs. The hardware and software of the DSP system in Fig. 5 are expanded to become a nine-phase control system. The nine-phase trapezoidal stator-current waveforms are generated similarly to the six-phase waveforms described in Section II. Based on the method presented in [17], the optimal (best) ratio of the number of field phases to torque phases

$$m = \frac{m_f}{m_t} \tag{12}$$

is calculated for the nine-phase machine as $m = 0.5$ (that is, $m_f = 3$ and $m_t = 6$), which is in contrast with $m = 1$ ($m_f = 3$ and $m_t = 3$) that is used in [16].

Fig. 8 shows a schematic of the experimental setup built to test the nine-phase induction machine. A three-phase 37-kW induction machine is used as a load drive because of its availability and lack of other means to load the multiphase machine. During testing, the induction-machine load drive is kept at a constant speed through the Powerflex 700 drive. The nine-phase DSP control system measures the rotor shaft speed, adds the slip speed for which the torque is to be measured, and then produces the PWM signals that drive the inverter. That way, the three-phase motor is used as load. It should be noted that, in this setting, torque is produced since the multiphase induction machine produces a torque that wants to increase the shaft speed while the three-phase motor keeps the shaft speed constant.

The torque is measured through a torque transducer installed on the shaft linking the two machines. An image of the test setup without the inverter and the DSP controller is shown in Fig. 9.

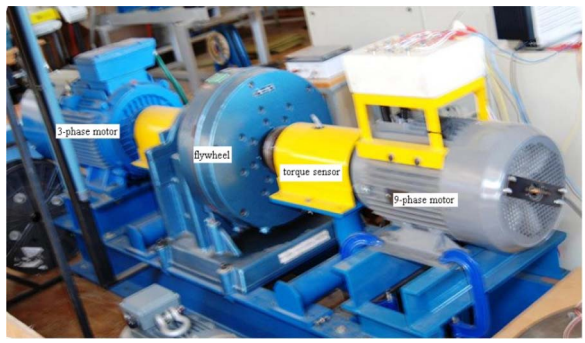

Fig. 9. Nine-phase induction machine on the test bench.

IV. Results

In Figs. 10 and 11, the measured stator-current waveforms of the nine-phase induction-machine drive at rated speed and flux and also at double rated speed and half rated flux are shown, respectively, for a single phase. With a flat-topped back-electromotive-force phase voltage of 400 V at rated frequency and flux and with $V_{\rm dc} = 400$ V, the drive shows good flux weakening operation (Fig. 11) just as in a brush dc machine. The current waveforms show that the current controller works well even at double rated frequency. Note that k of (11) is adjusted in the field-weakening speed range because of its dependence on the flux density.

In Fig. 12, the comparison of the measured and analytically calculated [using (10)] torque results of the drive is shown at rated field current $I_f = 5.83$ A and with a rated control gain value $k = 0.638$. In this measurement, the rotor speed is 500 r/min. From the figure, both results show a linear relationship between the torque current and the developed torque. Also, the figure shows that, at the rated torque current value ($I_t = 5.5$ A), the measured and calculated torque values are more or less the same. Nonetheless, the result shows that the drive maintains balanced MMF condition regardless of the torque current. This proves the BDCE operation of the machine.

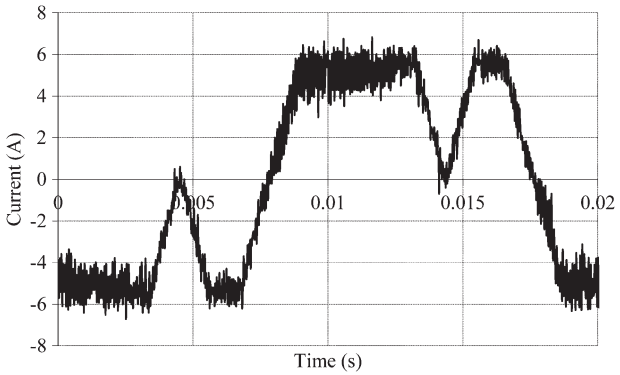

Fig. 10. Measured stator-phase current waveform of the nine-phase induction machine at a dc bus voltage of $V_{\rm dc} = 400$ V at rated flux, rated load ($I_f = 5.83$ A, $I_t = 5.5$ A, $k = 0.638$, and $T = 67$ Nm), $m = 3/6 = 0.5$, and rated speed (1500 r/min).

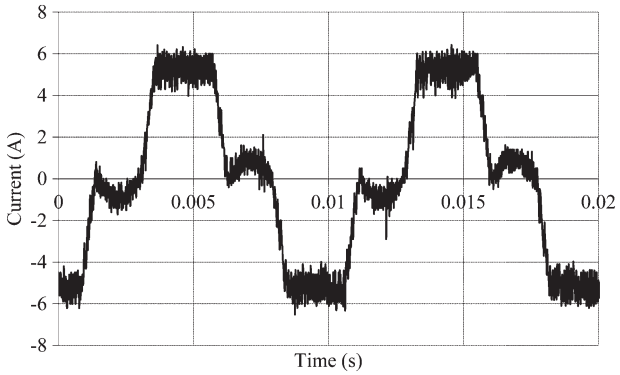

Fig. 11. Measured stator-phase current waveforms of the nine-phase induction machine at a dc bus voltage of $V_{\rm dc} = 400$ V in flux weakening at double rated speed (3000 r/min), $m = 3/6 = 0.5$, and half rated flux ($I_f = 1.1$ A, $I_t = 5.5$ A, and $k = 1.28$).

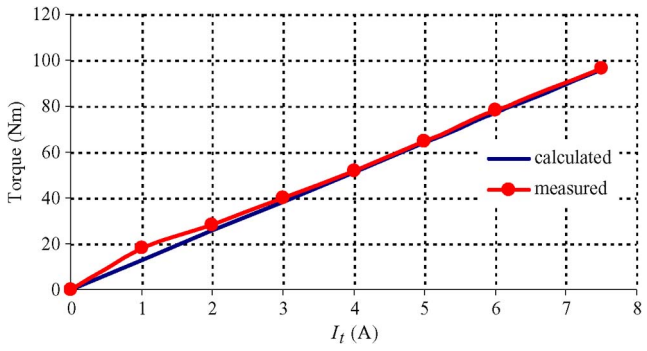

Fig. 12. Comparison of the measured and calculated torque versus torque current (I_t) with $I_f = 5.83$ A, $k = 0.638$, and speed = 500 r/min.

The linear relationship between the measured torque and torque current is achievable also at rated speed, as shown in Fig. 13. In this figure, there is a slight difference between the analytically calculated and measured torques. This may be a result of increased friction and windage losses and other stray-load losses; note that the analytically calculated torque is the developed torque while the measured torque is the shaft torque of the machine.

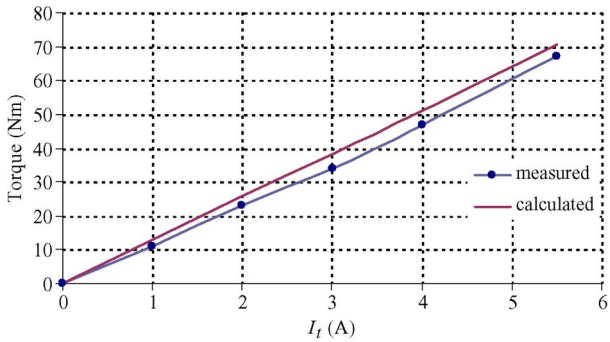

Fig. 13. Comparison of measured and calculated torques versus torque current with $I_f = 5.83$ A, $k = 0.638$, and speed = 1500 r/min.

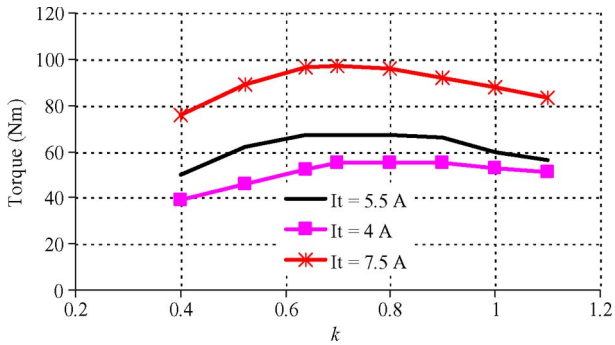

Fig. 14. Measured effect (at 500 r/min) of the k value (control gain) on torque with I_t as a parameter. The rated k value is $k = 0.638$, and the rated I_t value is $I_t = 5.5$ A.

The measured results in Fig. 14 show a low torque sensitivity to the k value for different torque currents, which is good, since k, from (11), is a function of rotor resistance which changes with temperature.

Similarly to dc drives, the output torque of the nine-phase induction-machine drive is proportional to the product of the air-gap flux and the torque-producing current, as given by (10). Therefore, the speed of the nine-phase induction machine can be increased above the rated speed while keeping the dc bus voltage constant and reducing the field current. The speed region above the rated speed is called the flux-weakening- or constant-power-speed region. This is because the machine torque falls in proportion with the flux, while the output power remains constant.

The relationship between the field current and the air-gap flux density is calculated from the method presented in [17]. As the speed (and frequency) increases above the rated speed (and rated frequency), then with field weakening, the flux density must change inversely proportional, i.e., to keep the voltage constant. Once the value of the flux density changes, the corresponding value of the field current required to produce the flux density is obtained from the graph.

The relationship between the air-gap flux density, control gain, k, and the field current of the machine versus frequency is shown in Fig. 15. The flux density is halved at double rated speed, and the relationship between flux density and field current is shown in the figure. The control gain k is inversely

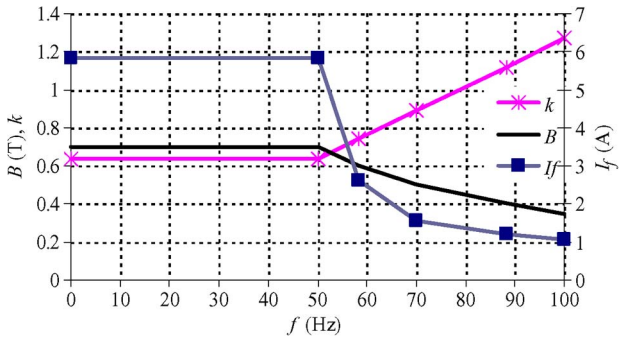

Fig. 15. Relationship between the air-gap flux density B, control gain k, and field current I_f versus frequency f.

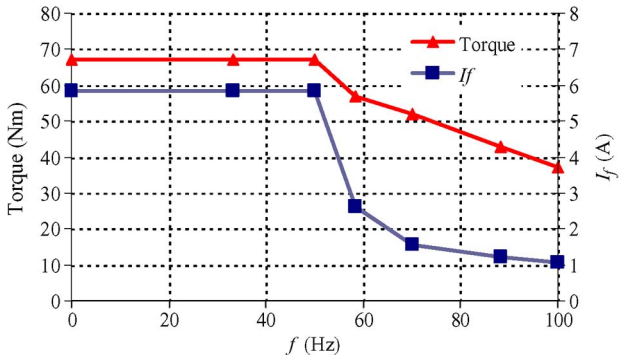

Fig. 16. Measured torque and field current versus frequency with $I_t = 5.5$ A.

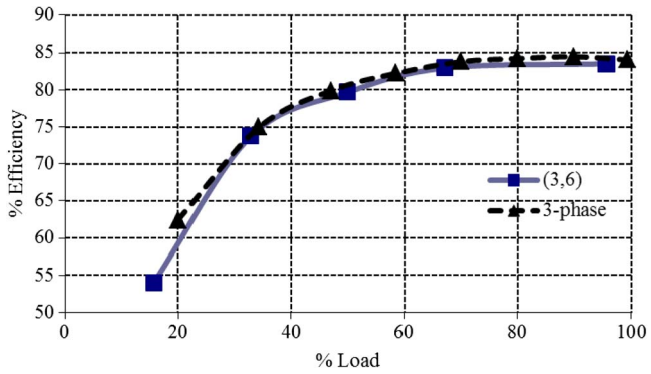

Fig. 17. Measured efficiency of the system (converter and induction machine) versus percentage torque load for the following: 1) $m = 0.5$ ($m_f = 3$ and $m_t = 6$) and 2) a standard 11-KW three-phase induction-machine drive under V/Hz control.

proportional to the flux density, as given by (11). The sharp decrease in the field current between 50 and 60 Hz is due to saturation.

In Fig. 16, the torque performance of the machine is verified at different frequencies. In this figure, the measured torque is shown with the appropriate field current in the flux-weakening-speed (frequency) region. This result further confirms the brush-dc compensating-winding operation of the control method. Fig. 17 shows the efficiency of the system (converter and induction machine). Also, in the figure, the 84% overall drive efficiency obtained at full load can be considered as very good compared with the 85% of the standard three-phase drive also shown.

V. Conclusion

The results in this paper proved that the proposed BDCE control method for multiphase induction-machine drives works remarkably well in the subbase and flux-weakening-speed regions of the drive. A linear relationship between the torque and torque current is found both in the analysis and through measurements. The current controller is effective even in the flux-weakening-speed region. The torque sensitivity to changes in the control gain are minimal, which is good since the control gain depends on the rotor-bar resistance which may vary by up to 40% due to temperature changes.

The phase current waveform used in the BDCE control method has a lot of Fourier series harmonics, but the combined phase currents generate a quasi-square air-gap MMF that rotate quite smoothly in time. From experimental tests, no more audible noise as from the three-phase drive was identified. The electromagnetic interference (EMI) from the inverter and machine cables is another study that must be conducted thoroughly to determine if there is more EMI.

Although, for the same power-rated induction machine, the insulated-gate bipolar-transistor (IGBT) count is much higher in the BDCE-controlled machine inverter and the current per phase is greatly reduced. Thus, the conduction and switching losses of each IGBT are reduced (switching losses are less as the IGBT can be switched at half the switching frequency with a full bridge), and thus, the total losses of all the IGBTs together will be the same as that of a three-phase inverter at the same power. In this paper, the measurement results showing the comparison of a nine-phase induction-machine system to a standard three-phase induction-machine system shows good efficiency of the BDCE-controlled machine.

The BDCE control method is suitable for very large drives utilizing high phase numbers because is it simpler to implement when compared with the increasing complexity of available control methods with an increase in the number of phases, e.g., up to 15 phases. As described in this paper, it has been proved that the BDCE control method can be used for cage-rotor multiphase induction machines.

Appendix

The following details give an interesting example of an enormous drive using standard IGBT switches from the shelf:

1) rated power: 45 MW;
2) number of phases: 15;
3) number of field phases (m_f): 3;
4) number of torque phases (m_t): 12;
5) power per phase: 3 MW;
6) IGBT switches: 4.5 kV/2000 A;
7) DC-bus voltage: $V_{\rm dc} = 0.75 \times 4.5$ kV $= 3.375$ kV;
8) rated field and torque phase currents:

$$I_f \approx I_t = \frac{3 \text{ MW}}{3.375 \text{ kV}} = 889 \text{ A}.$$

REFERENCES

[1] E. Levi, "Recent developments in high performance speed multiphase induction motor drives," in *Proc. 6th Int. Symp. Nikola Tesla*, 2006, pp. 53–64.

[2] G. K. Singh, "Multi-phase induction machine drive research—A survey," *Elect. Power Syst. Res.*, vol. 61, no. 2, pp. 139–147, Mar. 2002.

[3] H. A. Toliyat and T. A. Lipo, "Analysis of concentrated winding induction machines for adjustable speed drive applications-experimental results," *IEEE Trans. Energy Convers.*, vol. 9, no. 4, pp. 695–700, Dec. 1994.

[4] E. Levi, R. Bojoi, F. Profumo, H. A. Toliyat, and S. Williamson, "Multiphase induction motor drives—A technology status review," *Proc. Inst. Elect. Eng. —Elect. Power Appl.*, vol. 1, no. 4, pp. 489–516, Jul. 2007.

[5] A. C. Smith, S. Williamson, and C. G. Hodge, "High torque dense naval propulsion motors," in *Proc. IEEE IEMDC*, 2003, pp. 1421–1427.

[6] M. Jones, S. N. Vukosavic, and E. Levi, "Parallel-connected multiphase multidrive systems with single inverter supply," *IEEE Trans. Ind. Electron.*, vol. 56, no. 6, pp. 2047–2057, Jun. 2009.

[7] H. Xu, H. A. Toliyat, and L. J. Petersen, "Rotor field oriented control of five-phase induction motor with the combined fundamental and third harmonic currents," in *Proc. 16th Annu. IEEE APEC*, 2001, pp. 392–398.

[8] R. O. C. Lyra and T. A. Lipo, "Torque density improvement in a six-phase induction motor with third harmonic current injection," *IEEE Trans. Ind. Appl.*, vol. 38, no. 5, pp. 1351–1360, Sep./Oct. 2002.

[9] G. W. McLean, G. F. Nix, and S. R. Alwash, "Performance and design of induction motors with square-wave excitation," *Proc. Inst. Elect. Eng.*, vol. 116, no. 8, pp. 1405–1411, Aug. 1969.

[10] H. A. Toliyat, T. A. Lipo, and J. C. White, "Analysis of a concentrated winding induction machine for adjustable speed drive applications: Part 1 (motor analysis)," *IEEE Trans. Energy Convers.*, vol. 6, no. 4, pp. 679–683, Dec. 1991.

[11] F. Terrien, S. Siala, and P. Noy, "Multiphase induction motor sensorless control for electric ship propulsion," in *Proc. IEE PEMD*, Edinburgh, U.K., 2004, pp. 556–561.

[12] R. I. Jones, "The more electric aircraft: The past and the future?" in *IEE Colloq. Elect. Mach. Syst. More Elect. Aircraft*, 1999, pp. 1/1–1/4.

[13] M. J. J. Cronin, "The all-electric aircraft," *IEE Rev.*, vol. 36, no. 8, pp. 309–311, Sep. 1990.

[14] L. D. Lillo, L. Empringham, P. W. Wheeler, S. Khwan-On, C. Gerada, M. N. Othman, and X. Huang, "Multiphase power converter drive for fault-tolerant machine development in aerospace applications," *IEEE Trans. Ind. Electron.*, vol. 57, no. 2, pp. 575–583, Feb. 2010.

[15] U. C. Mupambireyi, N. P. van der Duijn Schouten, B. M. Gordon, and R. A. McMahon, "High phase number induction motor drives for battery applications," in *Proc. 8th Int. Conf. Power Electron. Variable Speed Drives*, London, U.K., 2000, pp. 229–234.

[16] Y. Ai, M. J. Kamper, and A. D. L. Roux, "Novel direct flux and direct torque control of six-phase induction machine with nearly square air gap flux density," *IEEE Trans. Ind. Appl.*, vol. 43, no. 6, pp. 1534–1543, Nov./Dec. 2007.

[17] N. Gule and M. J. Kamper, "Optimal ratio of field to torque phases in multi-phase induction machines using special phase current waveforms," in *Proc. ICEM*, 2008, pp. 1–5.

[18] L. Weichao, H. An, G. Shiguang, and S. Chi, "Rapid control prototyping of fifteen-phase induction motor drives based on dSPACE," in *Proc. ICEM*, 2008, pp. 1604–1607.

Nkosinathi Gule (M'11) received the M.Sc. (Eng.) degree from the University of Cape Town, Rondebosch, South Africa, in 2006 and the Ph.D. (Eng.) degree from Stellenbosch University, Stellenbosch, South Africa, in 2011.

He is currently a Lecturer with the Department of Electrical and Electronic Engineering, Stellenbosch University. His research interests are induction-machine drives and grid integration of renewable energy sources.

Maarten J. Kamper (SM'08) received the M.Sc. (Eng.) and Ph.D. (Eng.) degrees from Stellenbosch University, Stellenbosch, South Africa, in 1987 and 1996, respectively.

In 1989, he joined the academic staff of the Department of Electrical and Electronic Engineering, Stellenbosch University, where he is currently a Professor of electrical machines and drives. He is also a South African National Research Foundation-supported scientist. His research area is computer-aided design and control of reluctance, permanent-magnet, and induction electrical machine drives, with applications in electric transportation and renewable energy.

Prof. Kamper is a Registered Professional Engineer in South Africa.